TRANSLATIONAL
BIOPHOTONICS
Open Access

Fiber-based hand-held RCM-OCT probe for noninvasive assessment of skin lesions and therapy guidance

Gopi Maguluri | John Grimble | Mircea Mujat | Jesung Park |
Aliana Caron | Nicusor Iftimia 🆔

Physical Sciences, Inc., Andover, Massachusetts, USA

Correspondence
Nicusor Iftimia, Physical Sciences, Inc., Andover, Massachusetts, USA.
Email: iftimia@psicorp.com

Abstract

Noninvasive assessment of skin lesions, especially of basal cell carcinoma (BCC), has benefited more recently from the use of optical imaging techniques such as optical coherence tomography (OCT) and reflectance confocal microscopy (RCM). While RCM provides submicron scale resolution and thus enables identification of skin morphological changes of the skin, with the downside of limited penetration depth, OCT imaging of the same lesion brings the benefit of better resolving its depth of invasion. OCT and RCM can be used either individually or combined within the same instrument for the noninvasive diagnosis of non-melanoma skin cancers (NMSCs). Their combined use has shown to provide certain benefits such as better characterization of the lesion's margins, both in depth and laterally, as well as improved sensitivity and specificity, as previously demonstrated by our team. In this article we report a new "fiber-based" implementation of the second-generation RCM-OCT hand-held probe. The fiber-based implementation of both imaging modalities enabled the construction of a smaller footprint/lower weight hand-held probe. Its preliminary evaluation on the skin of healthy volunteers is reported here, demonstrating improved capabilities for resolving sub-cellular structures and image skin morphology with micron-scale resolution to a higher depth than in the previous implementation, while also enabling the construction of angiography maps showing vascular remodeling.
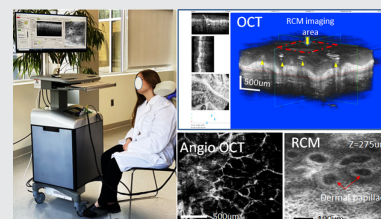
KEYWORDS

noninvasive evaluation, optical coherence tomography, reflectance confocal microscopy, skin lesions

INTRODUCTION

Optical coherence tomography (OCT) and reflectance confocal microscopy (RCM) are mature well-established optical imaging technologies in bioimaging [1, 2]. They are being used either independently or combined for the noninvasive diagnosis of various skin lesions, especially of nonmelanoma skin cancers (NMSCs) [3–10].

RCM imaging provides approximately 3 μm optical sectioning and 0.5 to 1.0 μm lateral resolution, with up to 300 μm imaging depth in skin [4, 7]. The resolution of RCM is on par with that of conventional pathology, which makes it a very good candidate for assessing various skin lesions [7]. RCM was proven to be effective in highlighting typical features for basal cell carcinomas (BCCs), such as nests of tumor, cell palisading, and clefting, with over 95% sensitivity and over 90% specificity [11, 12]. OCT imaging on the other hand has coarser scale resolution, with 5 to 10 μm optical sectioning resolution to depths of at least 1.5 mm. OCT has proven to differentiate reasonably well between the normal skin morphology and BCC tumor-related features, such as formation of round-shaped hypoechoic areas, often surrounded by a stronger signal (aura-like), caused by the high scattering of the stromal tissue around the tumor nodules [6, 11, 12]. However, when used alone, its specificity for diagnosing BCCs varied between 60% and 87% [13–15]. The three-dimensional (3D) rendering of the OCT data allows for building enface images at various depths, to at least 1.5 mm, that can be further processed (segmented) to identify the lateral and the deep margins of BCCs that were diagnosed with RCM [11, 12]. Therefore, OCT and RCM complement each-other, and when used together with the same instrument can help to improve BCC diagnosis, especially to evaluate their margins, as demonstrated recently by our clinical collaborators at Memorial Sloan Kettering Cancer Center (MSKCC) [11, 12, 16, 17].

The first-time implementation of RCM and OCT within a hand-held probe was demonstrated by our team in 2017 [11]. A T-shape telescope was used to combine OCT and RCM within the same optical path while preserving the imaging capabilities of each of the two technologies. This was possible by underutilizing the numerical aperture (NA) of the objective imaging lens in the OCT mode, while fully utilizing it in the RCM mode. Specifically, the custom-made water immersion objective lens had an NA of 0.8 in the RCM mode and 0.15 in the OCT mode. Although this probe was used in imaging over 250 patients to date, certain difficulties were encountered, which motivated the development of the second-generation probe. The first impediment was probe weight and size, as the laser illumination and detection modules were implemented within the probe. Second,

RCM alignment had some stability issues, as the optomechanics within the probe can get slightly misaligned over time. Third, the imaging speed of OCT was limited to 30 to 40 fps, and thus was too slow to build vasculature angiography maps, as faster B-scan repetitions are needed to assess speckle variance and detect blood movement through capillaries [18].

In this article we present a new fiber-based implementation of this probe, which addresses all the above-described limitations of the first generation probe, as well as its preliminary evaluation on healthy volunteers.

MATERIALS AND METHODS

The RCM-OCT instrument is composed of an instrumentation unit and a hand-held probe. The hand-held probe is connected to the instrumentation unit through electrical and fiber patch cords, 6 ft in length.

Hand-held probe

The simplified schematic of the hand-held imaging probe is shown in Figure 1A, while the CAD design and its implementations are shown in Figure 1B,C.

The backbone of the probe is a T-shape telescope (see lenses L1-L3) in Figure 1A, which combines the OCT and RCM beams within the same optical path using a dichroic mirror before reaching the custom-designed imaging objective (NA = 0.8, Photongear, Canada). The design of this probe enables separate manipulation of the imaging objective NA in each mode (see US Patent 9 655 521), and thus the preservation of the imaging capabilities of each of the two modes: submicron lateral resolution (∼0.9 μm) and optical sectioning on the order of 2.5 μm for RCM, with an imaging depth of ∼300 μm, and ∼10 μm lateral resolution for OCT with ∼1.2 mm imaging depth. The imaging objective has an entrance pupil of 9.2 mm, a focal length of 5.2 mm, a working distance of 1.5 mm, and the design was optimized for 830 nm to provide the best imaging performance in the RCM mode. The nominal imaging performance is <0.06 waves RMS axial at 830 nm.

The OCT and RCM imaging beams (1.31 μm/7.5 mW and 830 nm/1.5 mW, respectively) are sent from the instrumentation unit to the probe through fiber optic patch cords (SMF-28E fiber for OCT and double-clad DCF780S fiber for RCM). The light beams are then collimated using Thorlabs collimators (TC12APC-1310 for OCT and TC25APC-780 for RCM) and sent to two separate scanning engines. The OCT beam is scanned by a dual-axis MEMS mirror (Model A7B2-1, Mirrrorcle, California), while the RCM beam is scanned by an engine

consisting of a CRS12 kHz resonant scanner (Cambridge Technologies, Massachusetts), generating the line scan, and 7 mm aperture slow axis scanner (Model 6200H, Cambridge Technology, Massachusetts). The field of view (FOV) provided by this probe is 2 mm × 2 mm in the OCT mode and 0.70 mm × 0.70 mm in the RCM mode.

Imaging at different depths for RCM is enabled by a small stepper motor (model AM0820SB008008 + 08/1256:1 + MG09, MicroMO GmbH), which moves the position of objective lens relative to a stationary optically transparent cup-and-window, while the focus of OCT is handled by a liquid lens (Model D-A-39N1, Edmund Optics) over a range of ~1.5 mm. The cup-and-window is the only element of the probe that is in contact with the patient skin that gently flattens and stabilizes the imaged area. Index matching oil (n = 1.5) is applied to the skin surface to optically interface to the window and eliminate potential back-reflections, while ultrasound gel (n = 1.34) is used inside the cup as the necessary immersion medium for the objective lens.

The controllers for the resonant scanner, MEMS scanner, Z-focus motor, and liquid lens are integrated within the probe. A voltage regulator is placed as well inside the probe to regulate the voltages necessary for all these controllers.

The probe is 7.5 inches in length, 8 inches in height, and 4 inches in width. It weighs less than 1.5 lb, and
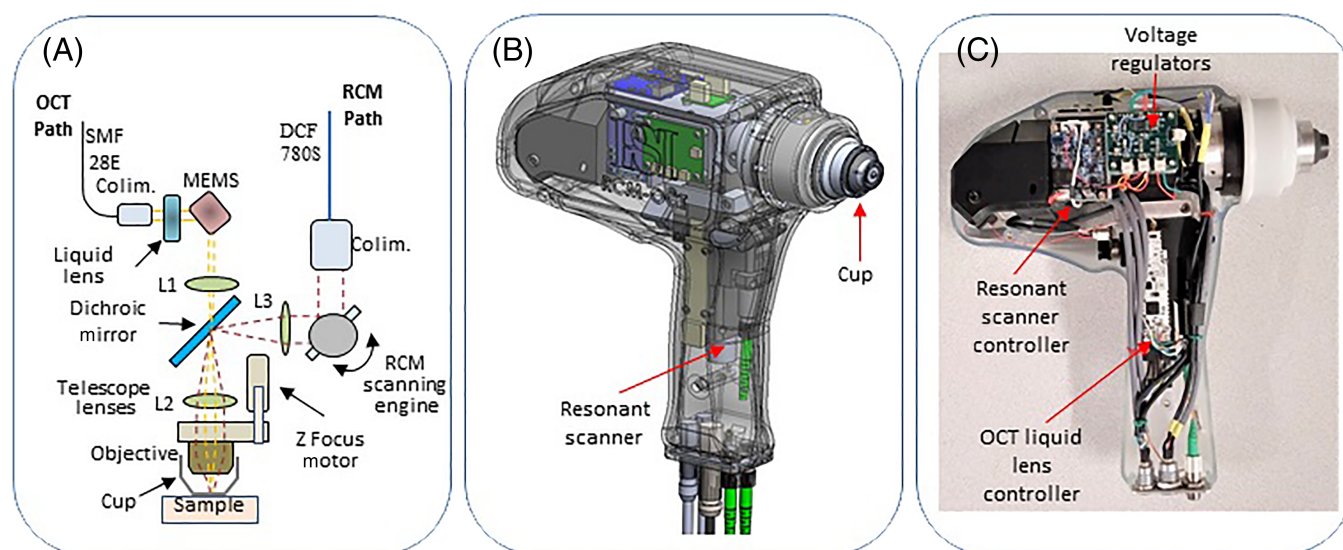
FIGURE 1   Hand-held probe design and physical implementation. (A) Simplified schematic; (B) CAD design; and (C) physical implementation.
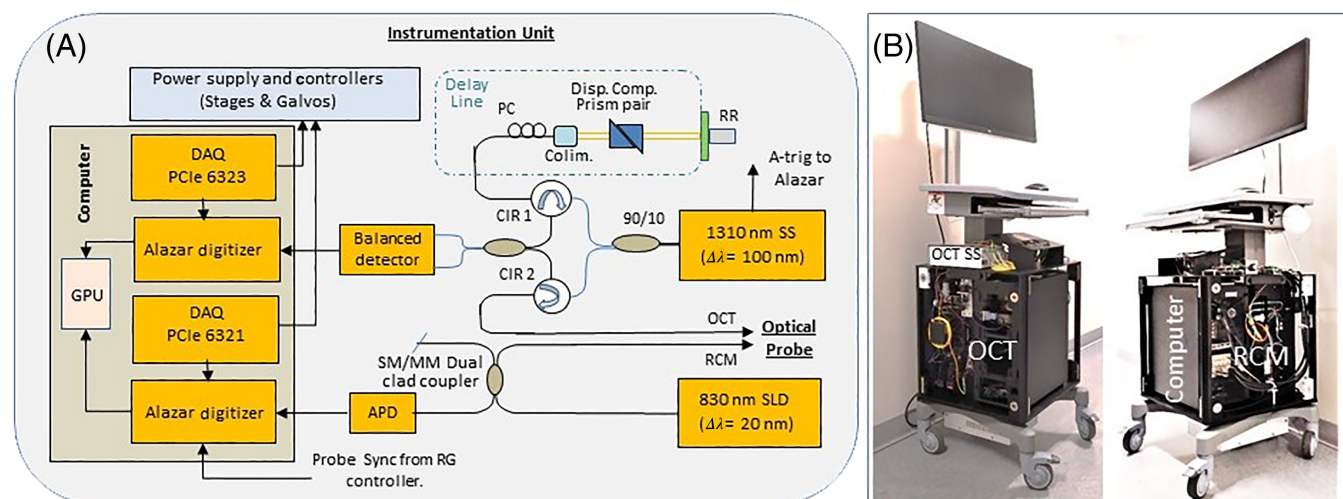
FIGURE 2   Schematic (A) and physical implementation (B) of the instrumentation unit. APD, avalanche photodetector; BS, beam splitter; CIR, circulator; DAQ, data acquisition card; GPU, graphical processing unit; PC, polarization controller; RR, retroreflector; SLD, superluminescent diode; SS, swept source.

therefore is relatively easier to operate than its predecessor, which weighted ~2.5 lb. The all fiber-optic configuration of this instrument allowed to detach the laser illumination and detection modules away from the probe head and place them into the instrumentation unit, making the probe lighter and smaller.

Instrumentation unit

The schematic of the instrumentation unit is shown in Figure 2A, while its implementation is shown in Figure 2B. The OCT subsystem, based on a swept-source approach, uses a fiber-optic interferometer, with the hand-held probe optics in the sample arm and an optical delay line in the reference arm. A MEMS-based swept source (Santec USA) with 100 kHz A-scan rate and a bandwidth of 105 nm with a central wavelength of 1310 nm is used for this system. The light is split in a 10/90 ratio and sent to the reference and sample arms of the interferometer, respectively. Two fiber circulators are used to maximize the return from both sample and reference arms of the interferometer.

A balanced detector is used to minimize swept source intensity noise. Signal fringes are digitized at a rate of 500 MS/s by a PCIe digitizer (AlazarTech, Model ATS 9352) and then processed in a GPU unit (NVidia, Model GTX 1060). A 4-analog output digitizer (National Instruments, Model PCIe 6323) is used to control the two axes of the MEMS mirror and the liquid lens. The liquid lens allows to adjust the focal plane of the OCT beam without affecting the position of the RCM focal plane.

The RCM subsystem uses a superluminescent diode as a light source with a central wavelength of 830 nm (Thorlabs, Model SLD830S-A10). The light is sent to the probe through a Single Mode/Multimode (SM/MM) double clad coupler (Thorlabs, Model DC780SEB). The inner core is used to send the light to the probe, while the double clad is used to collect and transmit the light to an avalanche photodetector (Model APD410A, Thorlabs). The signal is digitized by an Alazar digitizer (AlazarTech, Model ATS9146) with 125 ms/s digitization speed. A 2-analog output digitizer (NI PCIe 6321) is used to control the amplitude of the resonant galvanometer and the slow-axis galvanometer to generate RCM images. The Z-focus motor is controlled through the USB line.

The instrumentation unit, approximately $2 \times 2 \times 2$ ft in size, is placed on a wheeled cart, which also holds the monitor, the keyboard, and the mouse.

Instrument functionality and performance was first tested on resolution targets. The axial resolution of OCT subsystem was determined by measuring the coherence function when a partially reflecting target (microscope cover slip) was paced in the sample arm of the OCT system. An axial resolution of about 8 μm was obtained in air, which corresponds to about 6.01 μm in tissue. The theoretical resolution obtainable with the 105 nm bandwidth source is 7.2 μm in air. The relatively small discrepancy between the experimental and theoretical axial resolution was attributed to imperfect compensation of the dispersion between the two arms of the OCT interferometer. The lateral resolution of the RCM channel mode was measured using a high-resolution target, USAF 1951-1X. As observed in Figure 3, a lateral resolution better than 1 μm was observed. The second element of the group 9, which has a line width of 0.87 μm, was fully resolved.

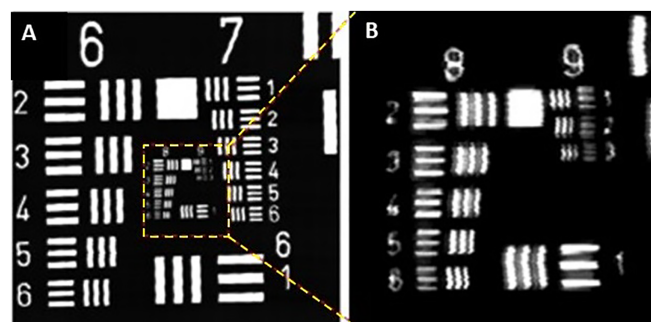The imaging speed and the resolution of the probe are summarized in Table 1.

FIGURE 3 RCM lateral resolution evaluation using the USAF1951-1X resolution chart

TABLE 1 Imaging probe performance

| Parameter	Imaging speed	Axial resolution	Lateral resolution	Obs.
OCT	50-67 fps, user selectable	8 μm	6 μm	OCT imaging speed: user controllable function of selected A-lines/frame[a]
RCM	12 fps	3.5 μm	0.87 μm	

[a]67 fps were obtained for a B-scan of 1492 A-lines.

FIGURE 4 Example of instrument testing on team members

FIGURE 5 Demonstration of the RCM/OCT imaging capabilities on a palm of a volunteer. (A) 3D OCT volume, with cross-sectional and enface views; (B,C) RCM images at various depths.
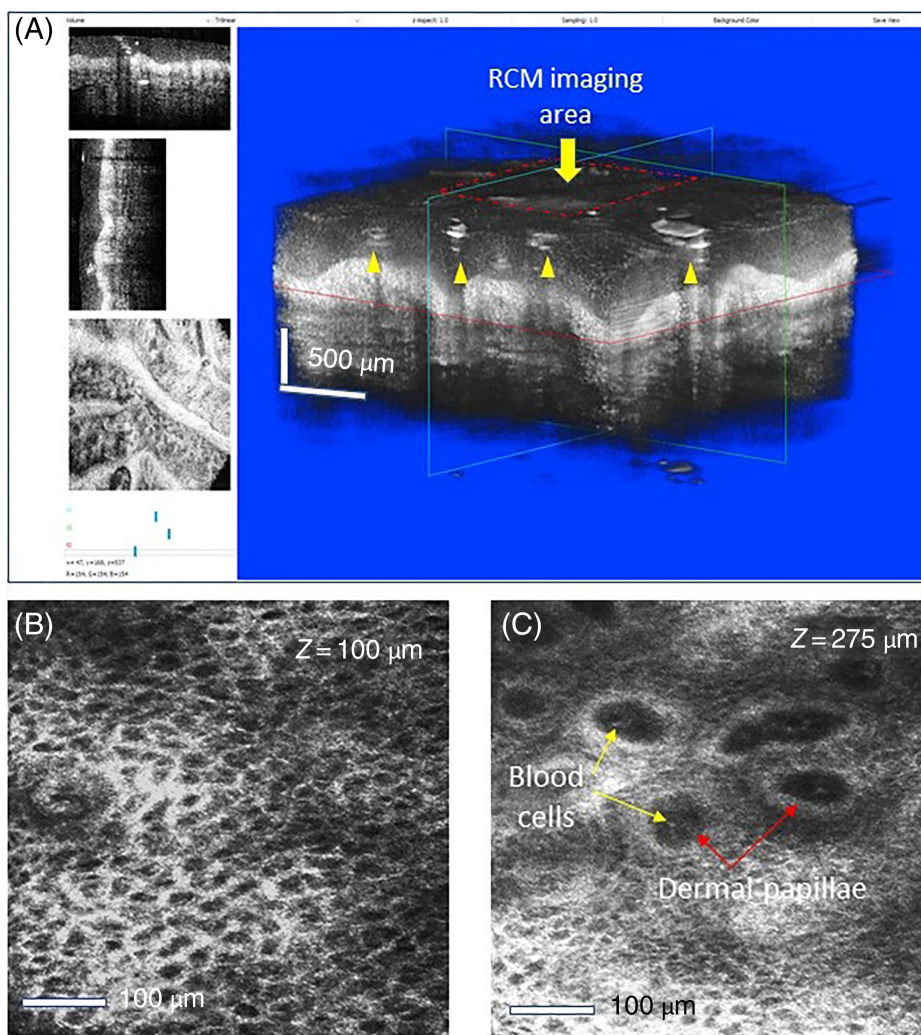
Data collection and processing

The instrument was preliminarily evaluated on the skin of team member (see example in Figure 4). Ultrasound gel was used between microscope objective and imaging cup to minimize light reflection on the glass/plastic surfaces, while microscope objective immersion oil was used between the cup and the skin. The imaging probe was held in place by a team member, while another team member was handling the data acquisition software. Spatially co-registered OCT scans were collected from different regions of skin. In this evaluation, three different acquisition modes were used: (a) OCT line scanning mode with associated RCM depth stack collection of 5 to 20 enface images at different depths up to 300 μm; (b) OCT raster mode (2 × 2 mm) and RCM enface at a fixed location, and (c) RCM enface at the basal layer and OCT raster data with three to five repeated B-scans in the same location to collect angiography data. The angiography images were processed by analyzing speckle variance [18] between consecutive three to five B-scans at a rate of 65 frames/s and averaging of the mean intensity projections.

RESULTS

Multiple RCM/OCT scans were collected from different skin areas of the volunteers to evaluate instrument capability for resolving tissue morphology including cell organization and vascular details. A representative OCT-RCM image collected from the palm of one of the volunteers is shown in Figure 5.

As it can be observed, the collected 3D OCT volumes can be used for displaying either cross-sectional images or enface images at different depths. The scan volume is 2 mm × 2 mm × 1.5 mm, as it can be observed in Figure 5A. The image processing software enables the display of cross-sectional images in two orthogonal directions of enface images at different depths of the 3D OCT volume data.

The high resolution of OCT is proven by its capability to resolve sweat glands, to visualize morphological details in different imaging planes, and to delineate dermal-epidermal junction. Simultaneously, spatially co-registered RCM images can also be collected at different depths, up to 300 μm. Figure 5B,C clearly demonstrates the capability of RCM to differentiate cells, blood vessels, and dermal papillae.

Another example showing skin morphology on the ventral side of the volunteer arm is shown in Figure 6. As it may be observed, the angiography map, collected by analyzing speckle variance of five consecutive OCT B-scans, shows detailed vascular morphology, while the RCM images collected at various depth up to 200 μm show fine cellular details and collagen structures. The RCM images collected at different depths clearly show
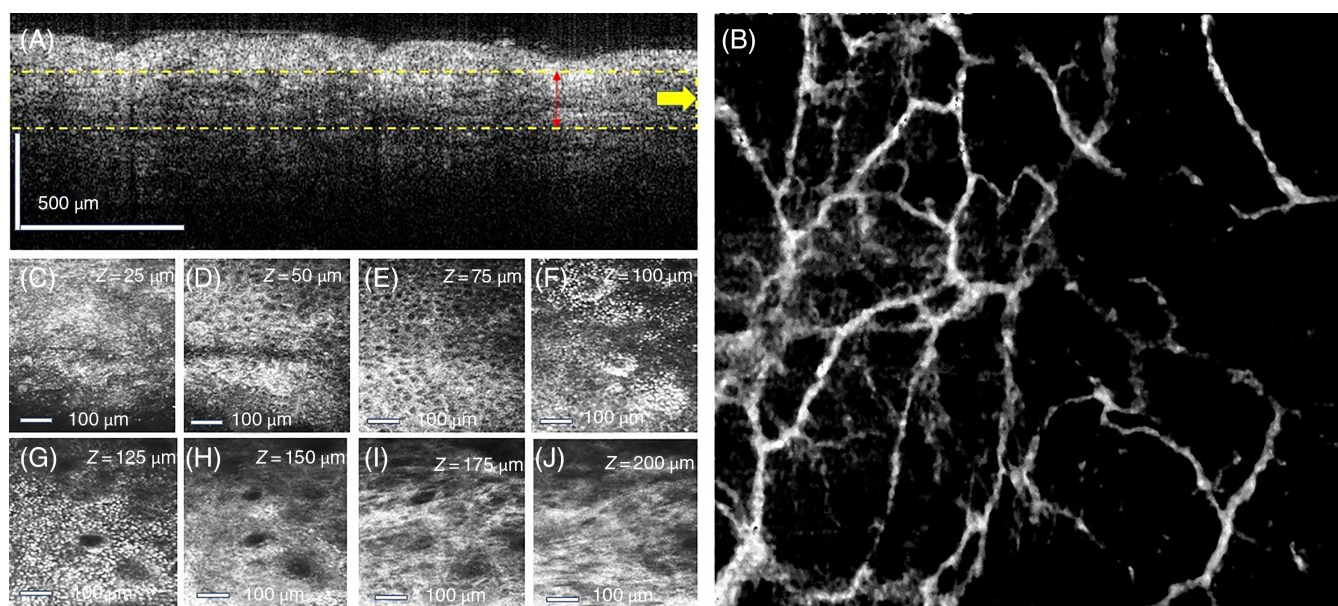
FIGURE 6 Demonstration of the RCM/OCT imaging capabilities on a volunteer's forearm. (A) 2D cross-sectional OCT image; (B) OCT angiography image showing vascular details at the dermal–epidermal junction; (C-J) RCM images collected at various depths showing different epidermal layers (stratum corneum, lucidum, granulosum, spinosum, and basale) and collagen structures in the upper dermis

the morphology of different skin layers: stratum corneum (Figure 6C), stratum lucidum (Figure 6D), stratum granulosum (Figure 6E), stratum spinosum (Figure 6F, G), stratum basale (Figure 6H), as well as the presence of the collagen fibers in the upper dermis (Figure 6I,J).

DISCUSSION

The implementation of RCM and OCT within a relatively low weight/small size probe was possible by using a fiber-based approach for both sample illumination and light collection in both imaging modes, as well as by detaching and placing the light detection modules out of the probe and into the instrumentation unit. Furthermore, the fiber-based approach made the RCM probe more robust than in the previous implementation, as the same fiber was used for both sample illumination and light detection. Our preliminary evaluation study, in which the probe was used over the course of 4 weeks imaging various skin locations on different subjects, did not show any changes in the RCM/OCT signal-to-noise-ratio (SNR) or imaging resolution. The measured OCT SNR was kept at over 108 dB (measured with a ND filter placed in the sample arm).

With further development to improve imaging speed from currently maximum 67 to 130 fps using a 200 kHz swept-source and the use of a C-based software, a more rapid analysis of OCT imaging results will be possible: display of 3D volumes and angiography maps within a few seconds after completing the 3D scan. All these features will widen clinical adoption and use of RCM/OCT for skin cancer diagnosis and therapy guidance.

The cost of the instrument is still a potential limitation to wide clinical adoption. The cost of the parts in the current implementation is approximately $50k for low fabrication volumes, governed mostly by the costs of the OCT digitizer (~8 k) and swept source laser (~18 k). However, these costs will significantly decrease for large volume production (>100 units).

The instrument is currently being used in a pilot clinical study at Memorial Sloan Kettering Cancer Canter (MSKCC), which has the goal of using RCM/OCT imaging to guide radiotherapy and laser ablation therapy of BCCs located on the hand and neck areas of the skin. We expect that the combined use of OCT and RCM within the same imaging probe will offer clear advantages, as compared to sequential use with following advantages: (a) spatial correlation of RCM and OCT will enable better identification of lesion margins, as previously demonstrated by our team [11, 12, 17]; (b) will simplify the imaging protocol and save considerable time for both clinician and patient, and (c) data processing and correlation of the imaging findings will provide a more comprehensive picture of the tissue morphological changes before and after therapy.

CONCLUSION

In conclusion, the feasibility of implementing a fiber based RCM/OCT imaging scheme within a hand-held probe has been demonstrated. The preliminary testing on volunteers has shown excellent imaging capabilities in both modes, as well high stability of the instrument. All epithelial layers have been clearly identified in the RCM images, while OCT images have demonstrated the capability of the instrument to detect fine morphological details within the skin, up to 1.5 mm in depth. The clinical utility of combined RCM/OCT for diagnosing NMSCs has been demonstrated in our previous studies, while its capability to guide nonsurgical therapy will be evaluated within the current study at MSKCC.

CONFLICT OF INTEREST
PSI has a patent on RCM-OCT: US 9655521.

DATA AVAILABILITY STATEMENT
The data that support the findings of this study are available on request from the corresponding author.

ORCID
Nicusor Iftimia https://orcid.org/0000-0002-7713-6972

REFERENCES

[1] W. Drexler, J. G. Fujimoto, *Optical Coherence Tomography-Technology and Applications*, 2nd ed., Springer International Publishing, Switzerland **2015**.

[2] A. Levine, O. Markowitz, *JAAD Case Rep.* **2018**, *4*(10), 1014.

[3] P. Guitera, G. Pellacani, C. Longo, S. Seidenari, M. Avramidis, S. W. Menzies, *J. Invest. Dermatol.* **2009**, *129*, 131.

[4] P. Guitera, S. W. Menzies, C. Longo, A. M. Cesinaro, R. A. Scolyer, G. Pellacani, *J. Invest. Dermatol.* **2012**, *132*(10), 2386.

[5] T. Hinz, L. K. Ehler, T. Hornung, H. Voth, I. Fortmeier, T. Maier, T. Höller, M. H. Schmid-Wendtner, *Acta Derm. Venereol.* **2012**, *92*, 132.

[6] J. M. Olmedo, K. E. Warschaw, J. M. Schmitt, D. L. Swanson, *Dermatol. Surg.* **2007**, *33*, 421.

[7] M. Rajadhyaksha, A. Marghoob, A. Rossi, A. C. Halpern, K. S. Nehal, *Lasers Surg. Med.* **2017**, *49*(1), 7.

[8] T. von Braunmühl, D. Hartmann, J. K. Tietze, D. Cekovic, C. Kunte, T. Ruzicka, C. Berking, E. C. Sattler, *J. Eur. Acad. Dermatol. Venereol.* **2016**, *30*(11), 1919.

[9] M. Boone, M. Suppa, M. Miyamoto, A. Marneffe, G. Jemec, V. Del Marmol, *Biomed. Opt. Express.* **2016**, *7*(6), 2269.

[10] M. R. N. Avanaki, A. Hojjatoleslami, M. Sira, J. B. Schofield, C. Jones, A. G. Podoleanu, *Appl. Opt.* **2013**, *52*(10), 2116.

[11] N. Iftimia, O. Yélamos, C. J. Chen, G. Maguluri, M. A. Cordova, A. Sahu, J. Park, W. Fox, C. Alessi-Fox, M. Rajadhyaksha, *J. Biomed. Opt.* **2017**, *22*(7), 76006.

[12] A. Sahu, O. Yelamos, N. Iftimia, M. Cordova, C. Alessi-Fox, M. Gill, G. Maguluri, S. W. Dusza, C. Navarrete-Dechent, S. Gonzalez, A. M. Rossi, A. A. Marghoob, M. Rajadhyaksha, C. S. J. Chen, *JAMA Dermatol.* **2018**, *154*(10), 1175.

[13] O. Markowitz, M. Schwartz, E. Feldman, A. Bienenfeld, A. K. Bieber, J. Ellis, U. Alapati, M. Lebwohl, D. M. Siegel, *J. Clin. Aesthet. Dermatol.* **2015**, *8*(10), 14.

[14] F. Adan, P. J. Nelemans, N. W. J. Kelleners-Smeets, J. P. H. M. Kessels, T. Brinkhuizen, K. Mosterd, *Br. J. Dermatol.* **2021**, *185*(5), 1065.

[15] W. Jerjes, Z. Hamdoon, D. Rashed, A. A. Sattar, C. Hopper, *Photodiagnosis Photodyn. Ther.* **2021**, *36*, 102493. https://doi.org/10.1016/j.102493.

[16] M. Gill, A. Sahu, C. A. Fox, M. Cordova, S. Gonzalez, N. Iftimia, S. Aleissa, C. Navarrete-Dechent, S. Dusza, A. Rossi, A. A. Marghoob, M. Rajadhyaksha, C. S. J. Chen, *J. Cutan. Pathol.* **2020**, *48*(1), 53.

[17] N. Iftimia, A. Sahu, M. Cordova, G. Maguluri, M. Gill, C. Alessi-Fox, S. Gonzalez, C. Navarrete-Dechent, A. Marghoob, C. S. J. Chen, M. Rajadhyaksha, *J. Cancer* **2020**, *11*(20), 6019.

[18] M. S. Mahmud, D. W. Cadotte, B. Vuong, C. Sun, T. W. H. Luk, A. Mariampillai, V. X. D. Yang, *J. Biomed. Opt.* **2013**, *18*(5), 050901.